Orissa Journal of Physics
ISSN 0974-8202

Vol. 31, No.2
August 2024
pp. 168-187

Photocatalytic Degradation of Chlorpyrifos and 2,4,5-trichlorophenoxy Acetic acid using Biosynthesized Ag/Cu-ZnO-biochar Nanocomposite

DEEPAK PATHANIA[1]†, RISHU KATWAL[2], ARUSH SHARMA[3], A.K. SRIVASTAVA[4], SARITA PATHANIA[5], AND RICHA KOTHARI[1]

[1]*Department of Environmental Science, Central University of Jammu, Bagla, Samba, Jammu & Kashmir - 181143, India*
[2]*Department of Chemistry, Sri Sai University, Palampur, Himachal Pradesh-176061, India*
[3]*Department of Chemistry, Baddi University of Emerging Sciences and Technology, Solan, Himachal Pradesh, India-173205*
[4]*Faculty of Engineering & Technology, Veer Bahadur Singh Purvanchal University, Jaunpur (UP)-222003, India*
[5]*Department of Zoology, Sardar Patel University Mandi, Himachal Pradesh, India, 175001*
†*E mail: deepakpathania@cujammu.ac.in*

Received: 19 Nov 2024, Revised 28 December 2024, Published 1 February 2025

Abstract: In the present study, photocatalytic performance of mesoporous Ag/Cu-ZnO/biochar (ACZ-B) nanocomposite has been investigated for the removal of chlorpyrifos (CP) and 2,4,5-trichlorophenoxy acetic acid (2,4,5-T) from water system under solar radiation. The texture and morphology of nanocomposite was determined by X-ray diffraction (XRD), Fourier-transform infrared (FTIR) spectroscopy, photoluminescence (PL) analysis, transmission electron microscopy (TEM), Brunauer-Emmett-Teller (BET), and Dynamic light (DL) scattering. The optical band gap of ACZ-B nanocomposite was observed to be 2.84 eV. The effect of various parameters such as photocatalyst dosage, pH, concentration, times were optimized. After 150 minutes of irradiation about 94% and 89% removal of CP and 2,3,5-T, respectively was recorded with synergistic adsorption and photocatalysis. The kinetic analysis confirmed the pseudo-first-order for the degradation of pollutant.

Keywords: Nanocomposite, Photocatalyst, Chlorpyrifos, 2,4,5 Trichlorophenoxy acetic acid.

1. Introduction

The development of agrochemicals has been increased after the Second World War in order to enhance the productivity and availability of food production. Agrochemicals are used to prevent, eradicate, repel, or mitigate pests in order to maximize crop output and productivity. Organophosphates and other chemicals have been widely used for crop protection against pests. Rachel Carson released the book "Silent Spring" in 1962, which addresses the risks and consequences of pesticides on human and environment. However, the environmental issues and public health concerns resulting from chemical pesticides have already been well recognized [1]. The extensive use of pesticides provides benefits, but they also pose many ill effects on human [2,3]. The majority of the agrochemical run-off to surface water bodies and entered groundwater, remained in the environment for an extended period, with less than 1% remaining to target. The National Water Quality Inventory 2002 reported that agrochemicals are the primary source of river and stream water pollution [4].

Pesticides are classified on the basis of their prospective to shatter living organisms including insecticides, herbicides, and fungicides. The acute poisonings caused by pesticides are associated with more than 250,000 deaths per year. 2,4,5-Trichlorophenoxyacetic acid is broadly used chlorophenoxy herbicides, in agriculture, structurally associated with chlorine or methyl-substituted ring attached with an aliphatic carboxylic acid moiety [5]. Between 1945 and 1989 in Wales, chlorophenoxy herbicide poisoning was the second leading cause of mortality from herbicide poisoning [6]. During the Vietnam War, the United States sprayed nearly 12 million gallons of defoliant orange agent (a combination of 2,4-D and 2,4,5-T) in Operation Ranch Hand. It has been linked to inconsistent liver disease in veterans from the United States [7]. Various potential toxicities of Agent Orange such as headache, hypotension, nausea, dizziness, myotonia, hepatic injury, abdominal pain, etc. In 1985, the EPA in the U.S. prohibited the uses of 2,4,5-T and the Rotterdam Convention refused all international trade of 2,4,5-T. After 1985, the use and sale of this herbicide in Canada were restricted [8-10].

Chlorpyrifos is the largest organophosphate insecticide used worldwide in term of volume and value [11]. Organophosphorus compounds are highly noxious and causes certain problems like asthma, cancer, diabetes, etc [12-15]. Chlorpyrifos is readily absorbed through the skin courses skin irritation and systemic intoxication [16]. Absorption of pesticides through

the skin may result in high toxicity which can harm the endocrine, respiratory, cardiovascular, neurological, and reproductive systems [17-27]. Gradually the use of agrochemicals is increasing worldwide and which results in contamination of water. Therefore, scientists are forced to track down more inventive and environmentally affable tools for the elimination of toxic agrochemicals. Several methods have been used for the removal of pesticides from water includes chemical oxidation with ozone, photocatalytic method, combined ozone and UV irradiation, Fenton degradation, biological degradation, ozonation, membrane filtration and adsorption [22, 28-30]. Adsorption and photocatalytic oxidation methods are now recognized as the best options for the degradation of pollutants.

Several metal/metal oxides composites such as Fe/ZnO, ZnO/$CoFe_2O_4$, Au/TiO_2, TiO_2/GO/$CuFe_2O_4$, TiO_2/Al_2O_3/G, and Fe_3O_4@ Ag_3PO_4 have been reported for the photodegradation of pesticides from the aqueous environment [28-33]. Many experts have attempted the utilizing of biomaterials for the degradation of agrochemical contaminants. The incorporating transition metals and metal oxides into biochar were found highly promising for pollutant removal [33].

Biochar (BC), a cost-efficient, carbon rich material produced in an oxygen-free environment by pyrolysis of biomass. Some desirable properties such as environmentally friendly, high porosity, high ion exchange capability, and oxygenated functionality make them a better agent for the removal of chemical contaminants from wastewater. Previously various studies have been reported on biochar-based nanocomposite and their utilization for water remediation [34-37].

Our main focal points are low preparation cost, low toxicity, and high stability of prepared nanocomposites for degradation of agrochemicals. Nanocomposite was characterized by techniques such as XRD, FTIR, PL TEM, BET, and DL. Different reaction parameters were optimized for photocatalytic effective degradation of pollutants.

2. Materials and methods

2.1. Collection of leaves

Diseases free fresh leaves of Melia azedarach were cleaned with distilled water many times and dried for 5 days at room temperature. The leaves

were then ground and dried in an oven for 24 hours at 600ºC. Now, leaves were pulverized and stored in an airtight container.

2.2. **Preparation of aqueous leaf extract**

It was prepared by boiling 6 g of leaves powder in 250 ml at 90 ℃ for 3 hours on stirrer using Soxhlet apparatus. It was then filtered, concentrated, and stored for future nanocomposite production.

2.3. Biosynthesis of ACZ-B nanocomposite

In this process, ACZ-B nanocomposite was prepared in two steps. The initial stage, 60 mL of 0.1M silver nitrate and 50 mL of 0.1M copper nitrate solution were added in a 250 mL beaker. Then 15 mL of leaf extract was added drop-by-drop while stirring continuously. This solution was agitated for 30 minutes at 55 ^{o}C using a magnetic stirrer. To above mixture 60 mL 0.1M zinc nitrate and 40 mL 0.2M sodium hydroxide were added with constant stirring. The mixture was agitated for two hours at 55 ^{0}C. The obtained precipitates were filtered, washed first with ethanol and distilled water (1:10) and then with distilled water many times. Then 1.5 g of activated biochar scattered in 50 mL double distilled water was added into the slurry of Ag/Cu–ZnO nanomaterials with constant stirring for 1 hour at 60 ^{0}C. The precipitates were filtered and oven dried for 24 hrs at 60 ^{o}C.

2.4. Photocatalytic degradation of agrochemicals

The agrochemicals degradation was evaluated by photocatalytic efficiency of ACZ-B nanocomposite for CP and 2,3,5-T as a targeted pollutant in water. The influence of photocatalysis was explored using equilibrium adsorption in the dark followed by photocatalysis and synergic adsorption and photocatalysis. For the experiment, the suspension of agrochemicals (100 ppm) and ACZ-B composite (100 mg) were stirred magnetically for controlled agitation [38]. During adsorption, the suspensions were retained in dark to establish adsorption-desorptionequilibrium of agrochemical molecule. After achieving the equilibrium, the suspension was exposed to sunlight directly for photocatalysis. The effect of the different condition was studied by compared theboth reaction set up. Now, 5 mL solutions were taken out at definite time periods, centrifuged and exposed for determination of absorbance at 450 nm in the double beam UV-Vis spectrophotometer. Triplicates of readings are taken.

3. Characterization

Perkin Elmer Spectrum RX-I Fourier transform infrared spectrophotometer in range between 4000 cm^{-1} and 400 cm^{-1} was used to know the function group in the nanocomposite. The crystallite size and phase purity of ACZ-B was determined by X-ray diffractometer using CuKα radiation. High resolution transmission electron microscopy (Techni G2 20 S-Twin) using the gold-coated grid was used to determine the size of nanocomposite. Ultraviolet Visible spectrophotometer was used to determine the absorption spectrum. The pH was measured by pH meter (ELICO model LI-617, India). The specific surface area was calculated using help of Brunauer–Emmett–Teller through N_2 adsorption-desorption isotherms.

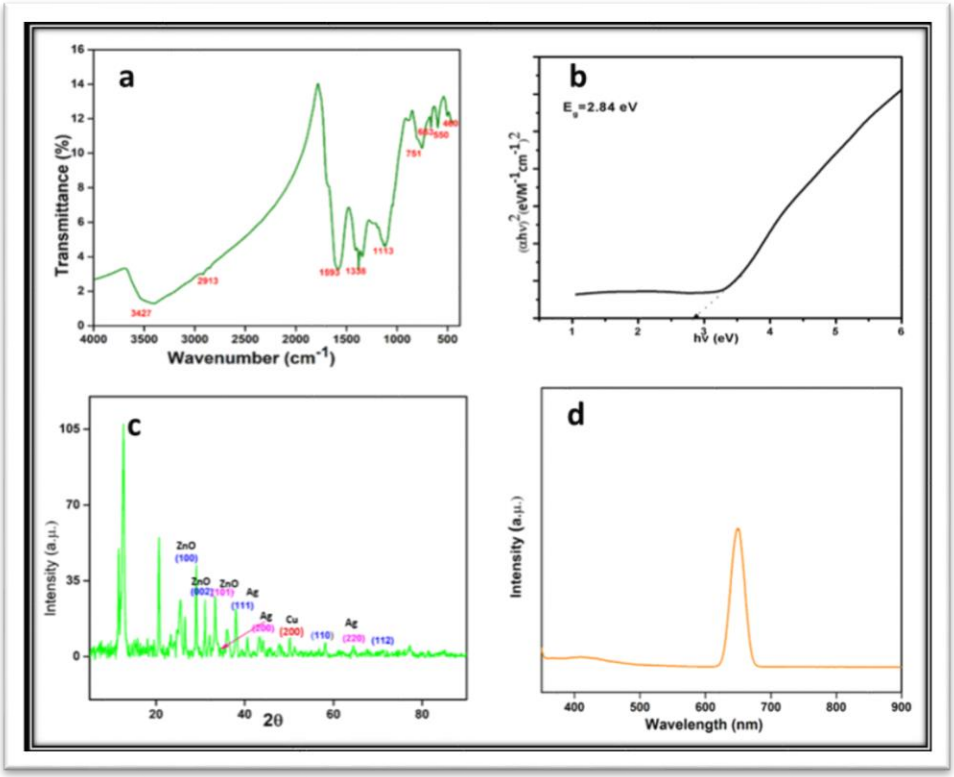

Fig. 1. ACZ-B nanocomposite (a) FT-IR spectrum (b) Band gap study (c) XRD (d) Photoluminescence study

4. Results and discussions

4.1 FTIR analysis

FTIR spectrum of ACZ-B nanocomposite is shown in Fig. 1a. Peaks at 3427, 2913, 1593, 1338, 1113, 663, 550 and 400 cm^{-1} were identified. Peak at 3427 cm^{-1} was inferred from stretching of O-H groups. Peak at 1593 and 1113 cm^{-1} were recorded due to C=O bond of carboxylic groups and stretching vibrations of C-C stretching of aromatic skeleton [39]. The broad peak at 2913 cm^{-1} was assigned to C-H vibration of aromatic compounds [40]. The peak at 1338 cm^{-1} was observed from C–H stretching, C–O stretching or CH_2 wagging. The peaks at 663, 550, and 400 cm^{-1} were recorded due to Zn-O vibrations [41,42].

4.2. Band gap study

The optical bandgap (Eg) energy of ACZ-B nanocomposite has been determined from a Tauc-plot as per equation (Eq. 1) as follow:

$$\alpha = \frac{A(h\nu - Eg)^{1/2}}{h\nu} \quad (1)$$

Where α is absorption coefficient, ν is frequency of light radiation, h is Planck's constant and Eg is band gap energy [43-45]. The band gap energy of nanocomposite was found to be 2.84 eV (Fig.1b).

4.3. XRD analysis

The purity and crystallinity of the synthesized ACZ-B nanocomposite was confirmed by X-ray diffraction. The XRD pattern of ACZ-B nanocomposite is shown in Fig.1(c). The crystallite size was calculated from Scherrer's formula as:

$$D = \frac{k\lambda}{\beta cos\theta} \quad (2)$$

Where k is constant, value of ≈0.90, β is the full width at half maximum (FWHM) of the peak, λ for Cu Kα is 1.5418 Å and θ is diffraction angle.

The XRD pattern was compared to the standard database and distinctive peak of copper was developed at 50.4°, which corresponds to the (200) crystal facets [46]. Furthermore, the emergence of peaks at 38.15°, 44.36°, and 64.53°, comparable to (111), (200), and (220) planes of silver (Ag), respectively indicated face-centered cubic structure [47]. The three characteristic peaks 31.6°, 34.4°, and 36.2° recorded for hexagonal wurtzite structure of ZnO matched to the crystal facets (100), (002), and (101) with the JCPDS, File No. 036-145145 [48]. The XRD pattern indicated the presence of copper, silver, and zinc oxide. The size of particles obtained from XRD data ranged between 15 nm and 20 nm.

4.4. Photoluminescence (PL) study

To study the recombination rate of photogenerated charge carriers and migration efficiency of ACZ-B nanocomposites PL technique was used. Fig.1d illustrates the photoluminescence spectra of ACZ-B nanocomposites. Broad bands were recorded at 600- 680 nm in the visible region [49]. ACZ-B exhibits a red emission at 660 nm due to the interstitial zinc transition and over-sufficiency of oxygen. The efficient charge separation and inhibition of electron-hole recombination enhances the photocatalytic activity. The deposition of Ag NPs onto the ZnO defect sites reduces the number of surface defects in ACZ-B nanostructures [50].

4.5. Brunauer-Emmett-Teller (BET) surface area analysis

The nitrogen adsorption/desorption isotherms and pore size distribution plot of the ACZ-B nanocomposite are shown in Fig. 2. Using BET surface area, the pore size distributions of the ACZ-B nanocomposite are shown in the inset of Fig. 3. The pore size of the ACZ-B nanocomposite was 2.49 nm. The ACZ-B nanocomposite confirmed type IV curve as appeared by a type H3 hysteresis loop.

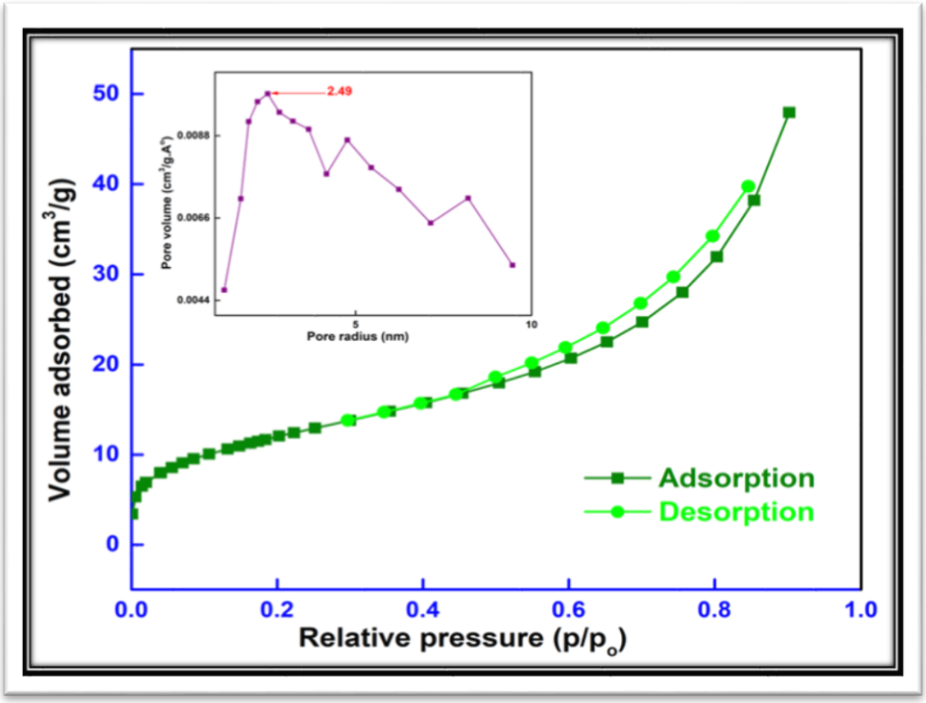

Fig. 2. N_2 adsorption/desorption isotherms and pore size distribution (inset) of ACZ-B nanocomposite

4.6. TEM Analysis

TEM results indicated the presence of needle shape particles distributed in biochar matrix with particle size ranged between 60 nm and 80 nm as shown in Fig. 3. The small aggregations arise in synthesized nanocomposite, which may be due to the hydrogen bonding between biomolecules and nature of the extract used as reducing agents.

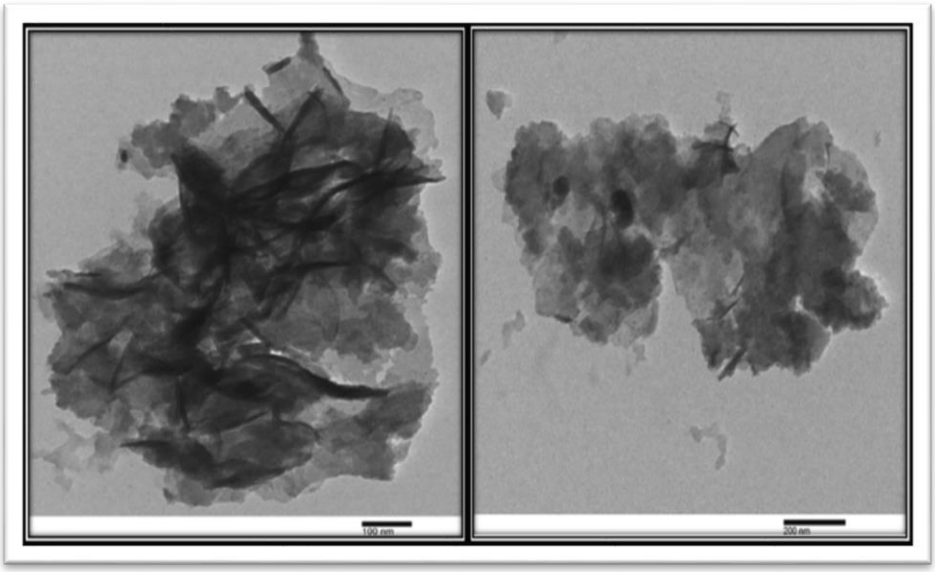

Fig. 3. TEM image of ACZ-B nanocomposite

5. Photocatalysis

The photocatalytic dehradation of ACZ-B nanocomposite was studied at two model targeted pollutants; CP and 2,4,5-T under different processes under direct-sunlight illustration (Figs. 4 and 5).

5.1. Adsorption in dark succeeded by solar light photocatalysis

In this process, the CP and 2,3,5-T solution containing the photocatalyst ACZ-B were stored in dark with continuous stirring for 1 hrs to establish adsorption/desorption equilibrium. For further photodegradation, the solutions were kept in sunlight. Figs. 4 and 5 depict the adsorption of CP & 2,3,5-T in the presence of ACZ-B photocatalyst.

Figures 4a and 5a indicating insignificant results of degradation by nanocomposite under adsorption in dark succeeded by photocatalysis. It was observed when solutions were kept in the dark containing ACZ-B nanocomposite only 14% and 24% of CP & 2,3,5-T were adsorbed within 90 mints of irradiation (Fig. 4a).

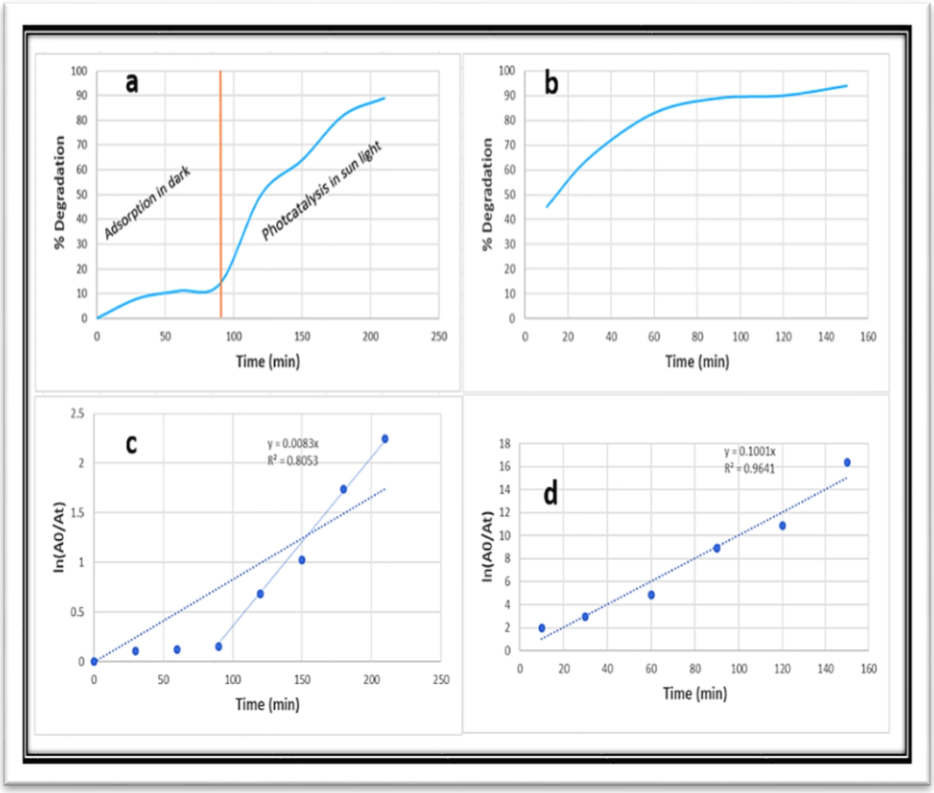

Fig. 4. Percentage degradation of chloropyrofors (a) adsorption in dark succeeded by photo catalysis and (b) synergic adsorption/photo catalysis; (c) pseudo-first-order kinetics for adsorption in dark succeeded by photo catalysis and (d) pseudo-first-order kinetics for photo degradation of chloropyrofors synergic adsorption/photo catalysis in presence of nanocomposite (initial concentration of chloropyrofors 100ppm, pH-6.7, temperature -30±5°C)

After, 210 minutes of sunlight exposure, 89% and 88% of CP and 2,3,5-T, respectively were degraded. When the solution is placed in the dark, it is likely that the surface of the nanocomposite is covered in pollutant molecules, preventing degradation. Furthermore, in presence of sunlight, an electron-hole pair was formed, which interacted with water and producing hydroxyl and superoxide radicals, therefore disrupting the mineralization of pollutants. ZnO nanoparticles had lower photocatalytic activity under sunshine as compared to nanocomposite. During photocatalysis the transition metal ions improves the absorption, interfacial charge transfers with the recombination of electron-hole pairs,

and significant increased the production of ·OH. The reduction and oxidation process is the main mechanism involving in photocatalytic reactions. The degradation rate (D) is calculated as (Eq. 3):

$$D=\frac{C_0-C_t}{C_0}\ X\ 100\% = \frac{A_0-A_t}{A_0}\ X\ 100\% \quad (3)$$

Where C_0 = initial amount of pollutants; C_t = Amount of pollutants at different time

A_0 = Initial absorbance; A_t = Absorbance at different time

The rate of photodegradation of pollutants was best fitted to pseudo-first-order kinetic model as follow (Eq. 4) [50].

$$\ln Ao/At = k_{app}\ t \quad (4)$$

Figs 5c and 6c show that photodegradation of pollutants follows Langmuir Hinshelwood model. The rate constants and R^2 of degradation of CP and 2,4,5-T are shown in Table 1.

5.2. Synergic Adsorption/Photodegradation by solar light

The synergic adsorption and photocatalysis was performed directly in presence of solar light. In this process the adsorption of pollutants onto the nanocomposite followed by photo degradation was observed. The photocatalytic degradation of 94% and 88 % was found for CP & 2,3,5-T after 150 min under synergic reaction as shown in Figs. 4b and 5b.

The pseudo-first-order kinetics was followed for CP & 2,3,5-T using ACZ-B nanocomposite as shown in Figs. 4d and 5d. The rate constant k and correlation coefficient (R^2) for CP & 2,3,5-T are shown in Table 1. The higher elimination of pollutants was obtained in synergic adsorption/photocatalysis due to brakeage of the molecules conjugation with superoxides. During synergic adsorption of agrochemical, absorption of light electron-hole pairs and free radicals generate simultaneously for breaking of the conjugation in the adsorbed and free molecules. The degraded product left the surface of adsorbent free and facilitate the photodegradation process by reduces the degradation time and increases the degradation rate.

The photocatalytic degradation of organic pollutants was due to oxidation reaction between photocatalyst and active species such as $OH^{\bullet}$, $O_2^{-\bullet}$ etc.

The mechanism for the degradation of pollutants is as follow:

ACZ-B+ Pollutants (P) → ACZ-B-P adsorbed (Sunlight)

ACZ-B(h^+)- P adsorbed + H_2O → ACZ-B($OH^{\bullet}$)-P + H^+

ACZ-B (h^+) –P adsorbed + OH^- → ACZ-B($OH^{\bullet}$)-P

ACZ-B(e^-) -P adsorbed + O_2 → ACZ-B ($O_2^{\bullet}$)-P

$O_2^{-\bullet}$ or $OH^{\bullet}$ + P-ACZ-B→ Intermediate Product → Degraded Product + Free ACZ-B

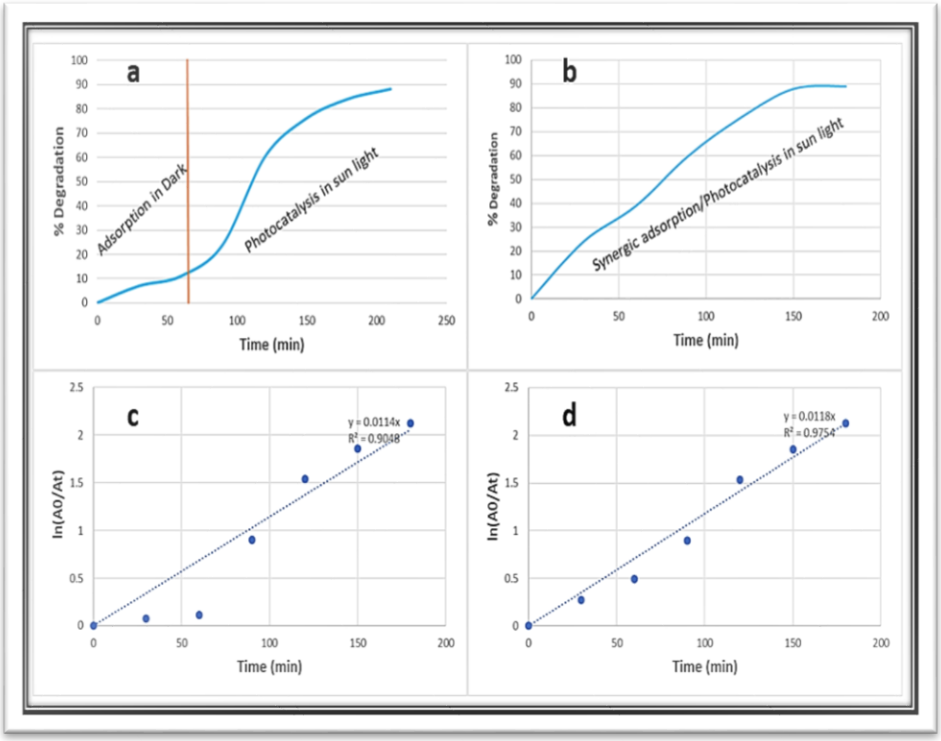

Fig. 5. Percentage degradation of 2,4,5-T (a) adsorption in dark succeeded by photo catalysis and (b) synergic adsorption/photo catalysis; (c) pseudo-first-order kinetics for photo degradation adsorption in dark succeeded by photo catalysis and (d) pseudo-first-order kinetics for photo degradation synergic adsorption/photo catalysis in presence of nanocomposite (initial concentration of 2,4,5-T 100ppm, pH-5.2, temperature -30±5°C)

Synergic adsorption and photocatalysis was found more proficient and effective compared with adsorption in dark succeeded photocatalysis process [51-54]. The outstanding degradation performance of nanocomposite improves its attributes for wastewater treatment.

6. Photocatalytic activities of ACZ-B nanocomposite on various parameters

6.1. Effect of photocatalyst dosage

The degradation of CP (40 mg/L) and 2,4,5-T (100 ppm) were carried out using various dosages of ACZ-B photocatalyst such as 0.025, 0.050, 0.075, 0.100, and 0.125g/L were illustrated under solar light using the

spectrophotometer (Fig.6a and 7a). The percentage of degradation was measured with the help of spectrophotometer. Based on the results it has been concluded that as the increase photocatalyst dosage, the percentage of degradation also increases. This could be explained due to the generation of the number of holes and radicals because the number of active photocatalytic positions increases, thus lead to faster degradation. Fig. 6a and Fig. 7a clearly show that 83% degradation rate at highest dosage 0.125g/L was observed in 2,4,5-T. Therefore, in CP as the photocatalyst dosage increases the degradation efficiency is reduced at high photocatalyst dosage. This could be happened due to excess use of photocatalyst, prohibits light penetration by reducing the transparency of the solution, reduced the process efficiency and eventually leads to a decrease in the percentage of degradation. Therefore, above results concluded that the better photocatalyst amount was considered for degradation of CP (0.100g/L) and 0.125g/L for 2,4,5-T [55-56].

6.2. Effect of concentration of pollutants

The concentration of CP and 2,4,5-T varied 20, 40, 60, 80, 100, and 120mg/L in a water solution containing 0.05 g of photocatalyst placed under solar light for 120 min and measured by the UV–Vis spectrophotometer (Fig. 7b and 6b). The results revealed that at a higher concentration of pollutants the degradation percentage decreased because as the contamination in water is too high, no adequate quantity of light reaches to photocatalyst to degrade the pollutants [57-58]. 20 mg/L and 50 mg/L are recorded to be optimized concentration of CP and 2,4,5-T.

6.3. Effect of pH

The degradation of pollutants were greatly affected by solution pH. The degradation of pollutants was investigated at varied pH at constant amount of photocatalytic (Figs. 6c and 7c). The degradation rate is low at high pH and, with low pH, the degradation rate high. In maximum 89% CP degradation was noticed at pH 6.7 and pH 5.2 maximum degradation was observed 73% for 2,4,5-T.

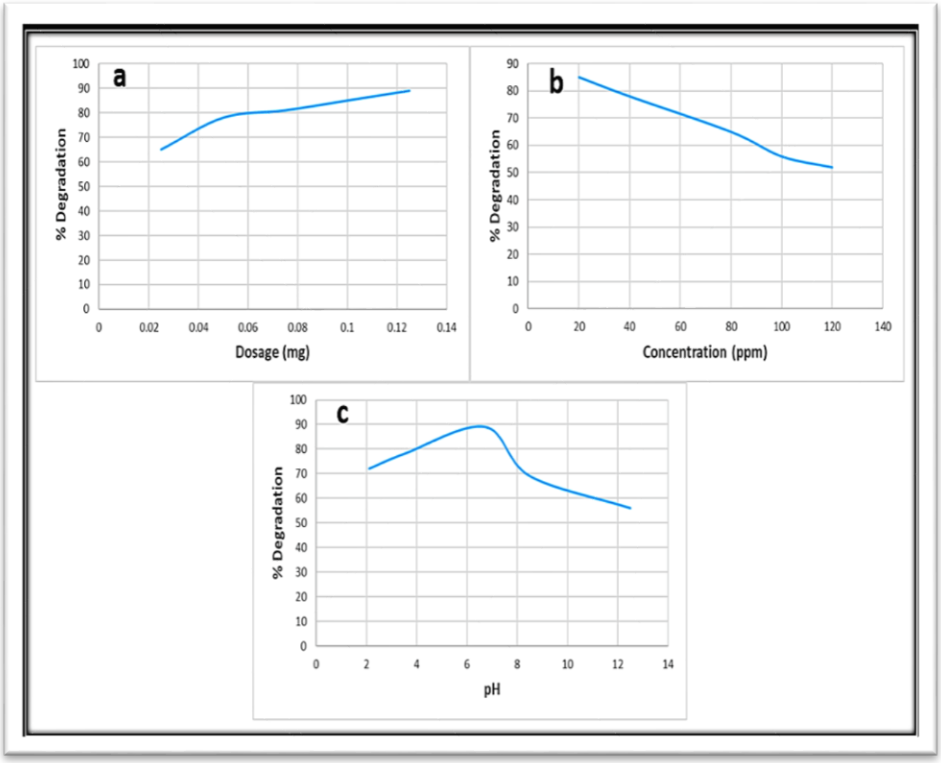

Fig. 6. Effect of reaction parameters on degradation of CP (a) effect of photo catalyst dosages (b) effect of CP concentration (c) effect of pH

6.4. Effect of time

The impact of time on the degradation of CP and 2,4,5-T employing ACZ-B photocatalyst in sunlight irradiation for 210 minutes under synergic reaction are shown in Figs. 4b and 5b. The degradation efficiency was gradually increasing with exposure time and degradation reached up to 94% and 88 % for CP & 2,3,5-T, respectively. The kinetic study at different interval of time followed pseudo-first-order.

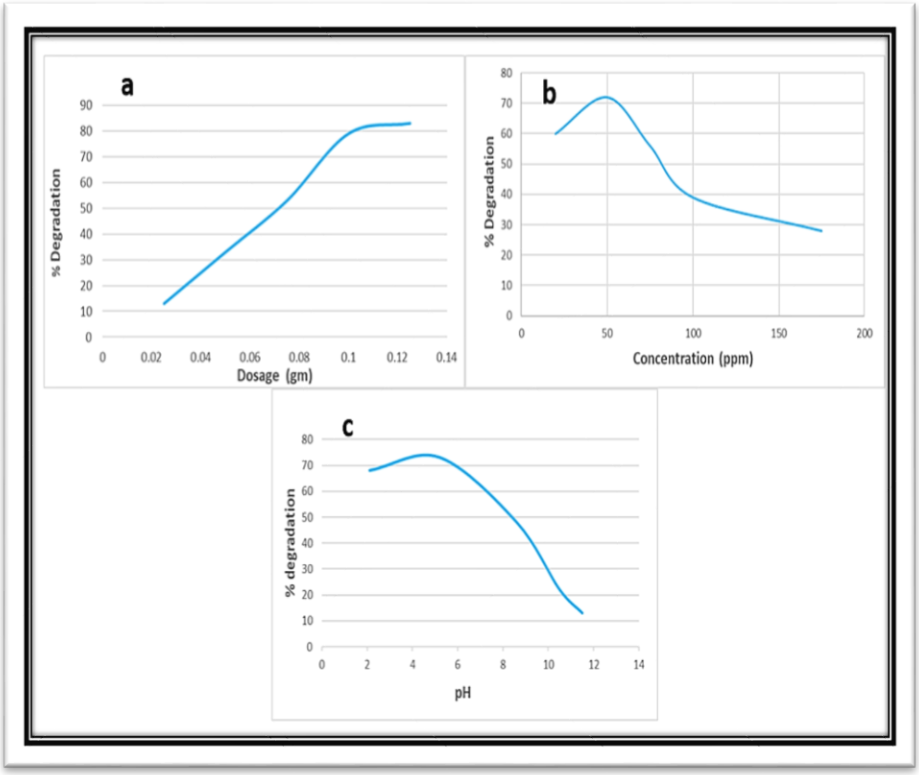

Fig. 7. Effect of reaction parameters on degradation of 2,4,5-T (a) effect of photo catalyst dosages (b) effect of 2,4,5-T concentration (c) effect of pH

7. Conclusion

The focus of this study was to achieve better photocatalytic performance by preparing Ag/Cu-ZnO-biochar nanocomposite *via* an easy, low-cost, green co-precipitation method. The exceptionally high degradation of 2,4,5-T as compared to CP were recorded by adsorption/photocatalytic process under solar illuminance. The parameters for photodegradation of pollutants including pH, photocatalyst dosage, and pollutant concentrations were optimized. TEM results inferred the formation of needle shape nanoparticles and high crystallinity. The present combination of biochar with transition metal and metal oxide has proven a better material for photocatalytic degradation of wastewater treatment.

CRediT statement

Deepak Pathania: Reviewing and Editing. Rishu Katwal: Reviewing and Editing. Arush Sharma: Writing of Original draft and Editing. Sarita Pathania: Writing and analysis. A.K. Srivastava: Supervision, Visualization. Richa Kothari: Supervision and Editing.

Acknowledgment

The Department of Environmental Sciences, Central University of Jammu, India, is acknowledged for offering the essential instrumental facilities for this research.

References

[1] G. R. Stephenson, Pesticide use and world food production: risks and benefits. In: Coats JR, Yamamoto H, editors. Environmental fate and effects of pesticides. ACS Symposium Series, Washington. 853 (2003) 261–70.

[2] A. Ozkara, Pesticides, environment pollution and health, Environment health risk- Hazardous factors to living species, 2016.

[3] IARC Monographs on the evaluation of the carcinogenic risk of chemicals to man. 15, (1977) 273-300. IARC, Lyons, France.

[4] U.S. Environmental Protection Agency. National Water Quality Inventory: Report to Congress, Reporting Cycle: Findings, Rivers and Streams, and Lakes, Ponds and Reservoirs, 2002.

[5] J. M. Bertolote, A. Fleischmann, M. Eddleston, D. Gunnell, Deaths from pesticide poisoning: A global response, Br. J. *Psychiatry.* 189(2006) 201-3.

[6] W. J. J. Hayes, Pesticides studied in Man, Williams & Wilkins, Baltimore, 1982.

[7] S. M. Bradberry, Mechanisms of toxicity, clinical features, and management of acute chlorophenoxy herbicide poisoning: a review. J. Toxicol. Clin. Toxicol. 38 (2000) 111–122.

[8] Study on the Calculation of the Benefits of Chemicals Legislation on Human Health and the Environment Development of a System of Indicators, Written by Marco Camboni, Anthony Footitt, Meg Postle, Theresa Fenn, Rebecca Halliday, Carl Clarke, Shaun da Costa, Abby Mahal (RPA), Anne Rathmann Pedersen, Dorte Rasmussen, Jens Torslov, 2016.

[9] K. Itoh, M. Kinoshita, S. Morishita, M. Chida, K. Suyama, Characterization of 2,4-dichlorophenoxyacetic acid and 2,4,5-trichlorophenoxyacetic acid-degrading fungi in Vietnamese soils.FEMS microbial. ecol. 84 (2013) 124-132.

[10] Unsworth- History of pesticide use. International Union of pure and applied chemistry (IUPAC), 2010.
[11] Environmental Protection Agency. Overview of the Ecological Risk Assessment Processin the Office of Pesticide Programs, U.S., Environmental Protection Agency. 2004.
[12] World Outlook of Chlorpyrifos 2011-2015, Reveals the Historical Development and Future Trend of Chlorpyrifos Industry by Continents & Countries.
[13] F. Van Der Berg, R. Kubiak, W. G. Benjey, M. S. Majewski, S. R. Yates, G. L. Reeves, J. H. Smelt, Emission of pesticides into the air. Water, Air & Soil Pollution. 115 (1999) 195-210.
[14] D. H. Lee, I. K. Lee, K. Song, M. Steffes, W. Toscano, B. A. Baker, D. R. Jacobs, A strong dose-response relation between serum concentrations of persistent organic pollutants and diabetes, Diabetes Care. 29 (2006) 1638-1644.
[15] E. L. Gunderson, FDA total diet study, April 1982-April 1984, dietary intakes of pesticides, selected elements and other chemicals, J. Assoc. Off. Anal. Chem. 71, 6 (1988) 1200-1209.
[16] Chlorpyrifos, Part 1: Toxicology, Journal of Pesticide Reform/Winter. 14 (1994) 4.
[17] T. K. Boucard, J. Parry, K. Jones, K. T. Semple, Effects of organophosphates and synthetic pyrethroid sheep dip formulations on protozoan survival and bacterial survival and growth, FEMS Microb. Ecol. 47 (2004) 121–127.
[18] A. M. Riederer, R. E. Hunter, S. W. Hayden, P. B. Ryan, Pyrethroid and organophosphorus pesticides in composite diet samples from Atlanta, USA adults, Environ. Sci. Technol. 44 (2010) 483–490.
[19] G. R. Oliver, H. G. Bolles, B. A. Shurdut, Chlorpyrifos: Probabilistic assessment of exposure and risk, Neurotoxicology. 21(2000) 203–208.
[20] J. D. Meeker, N. P. Singh, L. Ryan, Urinary levels of insecticide metabolites and DNA damage in human sperm, Hum. Reprod. 19 (2004) 2573–2580.
[21] W. Bicker, M. Lammerhofer, D. Genser, A case study of acute human chlorpyrifos poisoning: Novel aspects on metabolism and toxico-kinetics derived from liquid chromatography-tandem mass spectrometry analysis of urine samples, Toxicol. Lett. 159 (2005) 235–251.

[22] N. Tuzmen, N. Candan, E. Kaya, N. Demiryas, Biochemical effects of chlorpyrifos and deltamethrin on altered antioxidative defense mechanisms and lipid peroxidation in rat liver, Cell Biochem. Funct. 26 (2008) 119–124.

[23] A. Mehta, R. S. Verma, N. Srivastava, Chlorpyrifos-induced DNA damage in rat liver and brain, Environ. Mol. Mutagen. 49 (2008) 426–433.

[24] Q. Li, M. Kobayashi, T. Kawada, Chlorpyrifos induces apoptosis in human T cells, Toxicology. 255 (2009) 53–57.

[25] T. A. Slotkin, F. J. Seidler, Protein kinase C is a target for diverse developmental neurotoxicants: Transcriptional responses to chlorpyrifos, diazinon, dieldrin and divalent nickel in PC12 cells, Brain Res. 1263 (2009) 23–32.

[26] V. Scheil, A. Zurn, H. R. Kohler, R.Triebskorn, Embryo development, stress protein (Hsp70) responses, and histopathology in zebrafish (*Daniorerio*) following exposure to nickel chloride, chlorpyrifos, and binary mixtures of them, Environ. Toxicol. 25 (2010) 83–93.

[27] F. Xu, X. L. Chang, D. Lou, Q. Wu, Z. J. Zhou, Chlorpyrifos exposure causes alternation in dopamine metabolism in PC12 cells, Toxicol. Mech. Method. 22 (2012) 309–314.

[28] S. H. Khan, B. Pathak, M. H. Fulekar, Synthesis, characterization and photocatalytic degradation of chlorpyrifos by novel Fe: ZnO nanocomposite material, Nanotech. Environ. Eng. 3(2018).

[29] M. Naghizadeh, M. A. Taher, Ali-M. Tamaddon, Facile synthesis and characterization of magnetic nanocomposite ZnO/$CoFe_2O_4$ hetero-structure for rapid photocatalytic degradation of imidacloprid, Heliyon. 5 (2019) 2870.

[30] D. M. Fouad and M. B. Mohamed, Comparative Study of the Photocatalytic Activity of Semiconductor Nanostructures and Their Hybrid Metal Nanocomposites on the Photodegradation of Malathion,J. Nanomater.2012(2012) 524123.

[31] A. M. Ismael, A. N. El-Shazly, S. E. Gaber, M. M. Rashad, A. H. Kamel, S. S. M. Hassan, Novel TiO_2/GO/$CuFe_2O_4$ nanocomposite: a magnetic, reusable and visible-light-driven photocatalyst for efficient photocatalytic removal of chlorinated pesticides from wastewater this. RSC Adv. 10 (2020) 34806.

[32] N. R. N. Yusoff, C. Y. Peng, M. Yusoff, S. N. H. M. Nor, Photocatalytic degradation of metamifop using TiO_2/Al_2O_3/G

nanocomposite, AIP Conference Proceedings 2068, 020034 (2019).

[33] E. Shi, Z. Xu, W. Wang, Y. Xu, Y. Zhang, X. Yang, Q. Liu, T. Zeng, S. Song, Y. Jiang, L. Li, V. K. Sharma, Ag_2S-doped core-shell nanostructures of Fe_3O_4@Ag_3PO_4 ultrathin film: Major role of hole in rapid degradation of pollutants under visible light irradiation, Chem. Eng. J. 366 (2019) 123-132.

[34] K. W. Jung and K. H. Ahn, Fabrication of porosity-enhanced MgO/biochar for removal of phosphate from aqueous solution: application of a novel combined electrochemical modification method, Bioresour. Technol. 200 (2016)1029–1032.

[35] S. Khanchandani, S. Kumar and A. K. Ganguli, Comparative study of TiO2/CuS core/shell and composite nanostructures for efficient visible light photocatalysis, ACS Sustain. Chem. Eng. 4 (2016)1487–1499.

[36] Y. Lu, H. Yu, S. Chen, X. Quan, H. Zhao, Integratingplasmonic nanoparticles with TiO2 photonic crystal for enhancement of visiblelight-driven photocatalysis, Environ. Sci. Technol. 46 (2012)1724–1730.

[37] Z. Ding, Y. Wan, X. Hu, S. Wang, A.R. Zimmerman, B. Gao, Sorption of lead and methylene blue onto hickory biochars from different pyrolysis temperatures: Importance of physicochemical properties, J. Ind. Eng. Chem. Chem. 37 (2016) 261-267.

[38] D. Pathania, R. Katwal, G. Sharma, Mu. N. M. Rizwan Khan Ala'a H. Al-Muhtaseb, Novel guar gum/Al_2O_3 nanocomposite as an effective photocatalyst for the degradation of malachite green dye, Int. J. Biol. Macromol. 87 (2016) 366-374.

[39] Pyrolysis of Garden Waste: Comparative Study of Leucaenaleucocephala (Subabul Leaves) and Azadirachtaindica (Neem Leaves) Wastes: 7th Icon SWM—ISWMAW 2017, 2, 2019.

[40] A. T. Vu, T. N. Xuan, C. H. Lee, Preparation of mesoporous Fe2O3·SiO2 composite from rice husk as an efficient heterogeneous Fenton-like catalyst for degradation of organic dyes, J. Water Process. Eng. 28 (2019)169-180.

[41] H. Bouzid, , M. Faisal, F. A. Harraz, S. A. AlSayari, A. A. Ismail, Synthesis of mesoporous Ag/ZnO nanocrystals with enhanced photocatalytic activity, Catal. Today, 252, (2004) 20-26.

[42] S. Hayashi, N. Nakamori, and H. Kanamori, "Generalized theory of average dielectric constant and its application to infrared

absorption by ZnO small particles, J. Phys. Soc. Japan. 46 (1979) 176–183.

[43] J. Tauc, R. Grigovici, Liquid Semiconductors, Plenum Press, New York (1974) 159-220.

[44] Z. L. Wang, Nanostructures of zinc oxide, Mater. Today. 7 (2004) 26–33.

[45] C. N. R. Rao and A. Govindaraj, in Nanotubes and Nanowires, H. Kroto, P. O'Brien, and H. Craighead, Eds., The RSC Nanoscience and Nanotechnology Series, Royal Society of Chemistry, London, UK, 2005.

[46] D. Pathania, A. Sharma, L. Singh, S. Kumar, A.K. Srivastava, **Bio-synthesized Cu-ZnOhetro-nanostructure for catalytic degradation of organophosphate chlorpyrifos under solar illumination,** *Chemosphere,277, 130315, 2021.*

[47] F. A. Alharthi, A. A. Alghamdi, N. A. Zaqri, H. S. Alanazi, A. A. Alsyahi, A. E. Marghany, N, Ahmad, Facile one-pot green synthesis ofAg–ZnO Nanocomposites using potato peeland their Ag concentration dependent photocatalytic properties, Sci. Rep. 10 (2020) 20229.

[48] R. K. Shukla, N. Kumar, M. Pandey, Optical and Sensing Properties of Cu Doped ZnONanocrystalline Thin Films, J. Nanotechnol. 172864 (2015) 10.

[49] A. Modwi, K. K. Taha, L. Khezami, M. Bououdina, A. Houas, Silver decorated Cu/ZnOphotocomposite: efficient green degradation of malachite, J. Mater. Sci.: Mater. Electron.30 (2019) 3629-3638.

[50] A. Kumar, D.Pathania, N. Gupta, P. Raj, A. Sharma. Photo-degradation of noxious pollutants from water system using Cornulacamonacantha stem supported ZnFe2O4 magnetic bio-nanocomposite. Sustain. Chem. Pharm. 18 (2020) 100290.

[51] D. Pathania, A. Sharma, S. Kumar, A. K. Srivastava, A. Kumar, L. Singh. Bio-synthesized Cu-ZnOhetro-nanostructure for catalytic degradation of organophosphate chlorpyrifos under solar illumination. Chemosphere. 2021 130315.

[52] D. Pathania, M. Thakur, A. Sharma. Photocatalytical degradation of pesticides. InNano-Materials as Photocatalysts for Degradation of Environmental Pollutants 2020 (153-172). Elsevier.

[53] A. Sharma, S. Sood, D. Pathania. Remedial Role of Nanocomposite as Photocatalysts, Adsorbents, and Disinfectants in

Aqueous System and Their Biomedical Applications. In Metabolic Engineering for Bioactive Compounds 2017 (371-401). Springer, Singapore.

[54] D. Pathania, S. Dhar, A. Sharma, A.K. Srivastava. Decolourization of noxious safranin-T from waste water using Mangiferaindica as precursor. Environmental Sustainability. 2020,1-10.

[55] D. Pathania, A. Sharma, A.K. Srivastava. Modelling studies for remediation of Cr (VI) from wastewater by activated Mangiferaindica bark. Current Research in Green and Sustainable Chemistry. 2020, 3:100034.

[56] D. Pathania, A.K. Srivastava, A. Sharma. Bio-inspired fabrication of Cu–ZrO2 nanocomposites for the remediation of Cr (VI) from water system. Current Research in Green and Sustainable Chemistry. 2021, 4:100073.

[57] A. Sharma, K.K. Thakur, P. Mehta, D.Pathania. Efficient adsorption of chlorpheniramine and hexavalent chromium (Cr (VI)) from water system using agronomic waste material. Sustain. Chem. Pharm. 2018, 9:1-11.

[58] A. Sharma, Z.M. Siddiqui, S. Dhar, P. Mehta, D. Pathania. Adsorptive removal of congo red dye (CR) from aqueous solution by Cornulacamonacantha stem and biomass-based activated carbon: isotherm, kinetics and thermodynamics. Sep. Sci. Technol. 2019, 54(6):916-29.